Accepted Manuscript

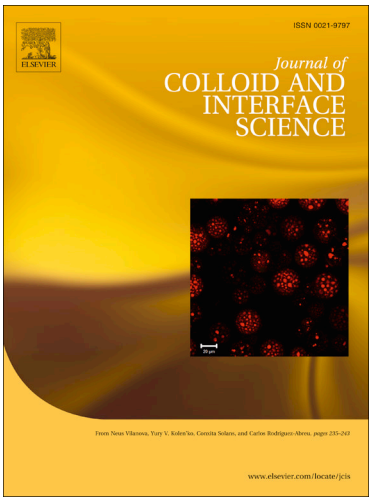

Epoxy-silica/clay nanocomposite for silver-based antibacterial thin coatings: Synthesis and structural characterization

Hugo Fernando Giraldo Mejía, Lucia Yohai, Andrea Pedetta, Karina Herrera Seitz, Raúl Ariel Procaccini, Sergio Antonio Pellice

PII: S0021-9797(17)30963-3
DOI: http://dx.doi.org/10.1016/j.jcis.2017.08.058
Reference: YJCIS 22705

To appear in: *Journal of Colloid and Interface Science*

Received Date: 2 May 2017
Revised Date: 16 August 2017
Accepted Date: 17 August 2017

Please cite this article as: H. Fernando Giraldo Mejía, L. Yohai, A. Pedetta, K. Herrera Seitz, R. Ariel Procaccini, S. Antonio Pellice, Epoxy-silica/clay nanocomposite for silver-based antibacterial thin coatings: Synthesis and structural characterization, *Journal of Colloid and Interface Science* (2017), doi: http://dx.doi.org/10.1016/j.jcis.2017.08.058

Epoxy-silica/clay nanocomposite for silver-based antibacterial thin coatings: Synthesis and structural characterization

Graphical abstract

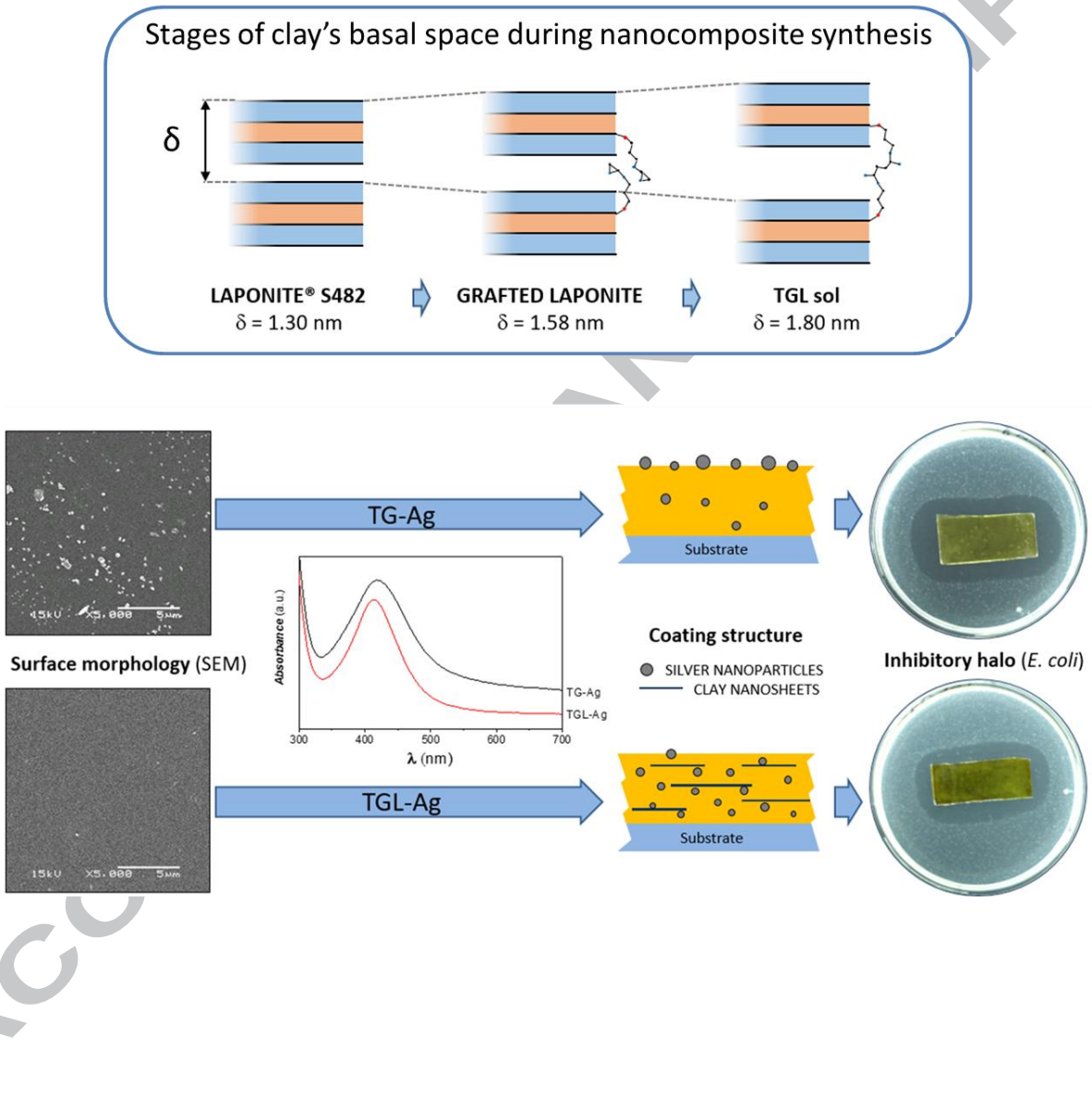

Epoxy-silica/clay nanocomposite for silver-based antibacterial thin coatings: Synthesis and structural characterization

Hugo Fernando Giraldo Mejía[1]*, Lucia Yohai[1], Andrea Pedetta[2], Karina Herrera Seitz[2], Raúl Ariel Procaccini[1], Sergio Antonio Pellice[1]

[1]*Instituto de Investigación en Ciencia y Tecnología de Materiales (INTEMA), CONICET-UNMdP, Av. Juan B. Justo 4302, B7608FDQ Mar del Plata, Argentina.*

[2]*Grupo Quimiotaxis, Instituto de Investigaciones Biológicas (IIB), CONICET-UNMdP, Casilla de Correo 1245 (7600) Mar del Plata, Argentina*

*Corresponding author: H.F. Giraldo Mejía
E-mail address: hgiraldo@fi.mdp.edu.ar. Postal address: Av. Juan B. Justo 4302, B7608FDQ Mar del Plata, Argentina. Telephone: +54 223 4816600, extension: 238.

Abstract

Development of new functional coatings in the field of health care, as antibacterial applications, deals with a straight control of the diffusive properties that rules the releasing of the active component. In this work, the development of a silver-rich nanocomposite thin coating, loaded with organically modified clay nanoparticles, is presented. The synthesis process included an environment-friendly silanization process of clay nanoparticles (Laponite® S482) with (3-glycidoxypropyl)trimethoxysilane (GPTMS) and the further hydrolytic condensation with tetraethoxysilane (TEOS). Silanization process and the obtained coatings were analysed by Fourier transformed infrared spectroscopy, UV-visible spectroscopy, X-ray diffraction, thermogravimetric curves and scanning electron microscopy. The silanization process of clay nanoparticles with the organically reactive alkyl alkoxysilane, allowed to stabilize and exfoliate the clay nanosheets within a hybrid organic-inorganic sol-gel material. Ring opening of grafted epoxy groups carried to an increasing of the basal spacing, of intercalated clay nanosheets, from 1.3 to 1.8 nm. Moreover, incorporation of organically modified clay nanosheets introduced a significant stabilization on the development of silver nanoparticles inside the structure of the nanocomposite coating, retaining the silver inside the coating material and restricting the growing of silver nanoparticles on the surface of the coating. Antibacterial behaviour, against *E. coli* cultures, performed through agar diffusion tests, provided promising results that allow assuming that the studied nanocomposite coating serves as a reservoir of ionic silver, permitting the antibacterial effect.

Keywords: Nanoclay, Grafted Laponite, Sol-gel, Hybrid Matrix, Silver Nanoparticles.

1. Introduction

In the past thirty years, the research work referred to epoxy clay nanocomposites had an interesting development due to the improvement of mechanical, structural and barrier properties.[1–3] Montmorillonite, natural clay with structural advantages like a hydroxyl reactive groups, exchangeable interlayer cations, Lewis acidity, high superficial area and expandable-layered crystal structure, is one of the most common minerals used in those works.

In case of materials with straight dimensional limitations as thin coatings, the use of nanoclays, with 1 nm in thickness, is a clear alternative as a key component for the development of functional nanocomposites [4–7]. The use of this kind of nanoparticles can avoid the structural damage caused when the size of particles is in the same order of magnitude than the thickness of the coating that contains them. In addition, the high exfoliation of the particles of Laponite® S482 avoids the formation of large agglomerates of particles that could have a similar effect on the integrity of the layer. Certainly, Naderi et al. observed a clear synergistic effect in the efficiency of anticorrosive coatings promoted by the insertion of clay nanoparticles in sol-gel formulations [8]. Laponite® S-482 is a synthetic clay that can be dispersed and exfoliated in aqueous solutions thanks to the incorporation of (1-hydroxyethylidene)bisphosphonate as a stabilizing agent. The hydrophilic clay platelets can be functionalized by silane grafting technique in order to increment the basal spacing, form steric barriers and avoid degelation process by reducing the disk-edge interactions in solution. This chemical modification can be produced by condensation reactions of alkoxysilanes on the reactive points like Si-OH or Mg-OH bonds available at the edges of clay platelets. Usually, silanization process of clays is performed in dry media by use of organic solvents as dispersing agents [9–11]. Then, this synthesis route allows a chemical matching between the inorganic clay nanoparticles and different organic-rich matrixes. Those properties make Laponite® S482 a suitable material for its incorporation in sol-gel formulations.

On the other hand, the development of hybrid organic-inorganic sol-gel coatings with application in industrial or health fields, were the ionic diffusion of functional components is required, it is essential the control of diffusive and barrier properties. It is the case of silver-doped sol-gel coatings with antibacterial properties. Antibacterial properties of silver lie in the ability of its ions to damage the cytoplasmic membrane and the respiratory enzymes of bacteria [12]. Nevertheless, the ionic mobility of silver could be extremely fast in sol-gel matrixes, which mean a strong antibacterial behaviour but only at short term [13–15]. So, introduction of clay nanoparticles could substantially improve the antibacterial behaviour of this kind of antibacterial coatings through the control of size and shape of silver nanoparticles and the ionic release behaviour [16].

The aim of the present study is to advance in the development of a novel thin antibacterial coating, with effectiveness at long term, based on silver releasing. The efficient use of exfoliated clay nanosheets, organically modified through a simple and environment-friendly method, is considered as a fundamental alternative in order to achieve the objective. In this sense, a silanization process for exfoliated clay nanosheets, in wet conditions, is analysed. This combination of the sol-gel chemistry with the knows effect of clay nanosheets on the stabilization of silver nanoparticles and the limitation that

they introduce in the ionic mobility, in order to produce thin coatings with improved antibacterial properties, represent a novel approach attending to the health care. Therefore, in this work, the silanization process of Laponite® S482 with (3-glycidoxypropyl)trimethoxysilane (GPTMS) in aqueous-alcoholic media and its effect on the structural properties of silver-doped hybrid organic-inorganic thin coatings is presented. The synthesis process and the structural properties of the developed coatings were analysed through X-ray diffraction (XRD and GIXRG), Fourier transform infrared spectroscopy (FTIR), thermogravimetric analysis (TGA) and scanning electron microscopy (SEM). In addition, the evaluation of the stability of precursor sols was performed by viscosity measurements. On the other hand, the aggregation state of silver in the nanocomposite coatings was studied by the Scherrer's formula analysis and their plasmonic bands in the UV-vis absorbance spectra. Finally, the antibacterial behaviour was analysed against *E.coli* cultures.

2. Experimental

2.1. Materials and synthesis method

Synthetic clay nanoparticles, chemically coordinated with (1-hydroxyethylidene)bisphosphonate [17] (Laponite® S482), were dispersed in aqueous-ethanolic media and exposed to a grafting process with (3-glycidoxypropyl)trimethoxysilane (GPTMS, Aldrich 99 %), the pH of the solution was adjusted with an acid solution to neutrality. The reaction proceeded under ultrasonic agitation and neutral pH. The resulting grafted nanoclay suspension was then mixed with tetraethoxysilane (TEOS, Aldrich 98 %) keeping a molar ratio GPTMS/TEOS = 40/60 and 2 wt. % of clay in respect to condensed silica, *i.e.*, an initial Laponite/silanes ratio of 0.52 wt. %. Hydrolytic condensation of the alkoxy groups from non-reacted GPTMS and TEOS, and the opening of epoxy rings, was performed by addition of concentrated nitric acid (HNO_3) under vigorous stirring at 1200 rpm and 25°C. Ag^+ ions were further added, at a molar ratio Ag/Si = 3/97, from a previously prepared ethanolic solution through silver nitrate ($AgNO_3$) and pyridine as stabilizer (2.85 % v/v of Pyridine and 5.91 %w/w of $AgNO_3$). The molar ratio Ag/Si was chosen based on previous works [15]. For comparative purposes, sols without clay nanoparticles and without silver doping were alternatively synthetized. Then, four kind of precursor sols were obtained: a basis matrix sol from TEOS and GPTMS (TG), a basis sol with clay nanoparticles (TGL), a basis sol with clay nanoparticles and silver doping (TGL-Ag) and a basis sol with silver doping (TG-Ag).

In order to evaluate the grafting process, portions of as-received and grafted clay were dried at 100°C to evaporate residual solvents and non-grafted GPTMS. On the other hand, through the dip-coating process at a withdrawal speed of 30 cm/min, the precursor sols were deposited onto microscope glass slides. After drying at room temperature, nanocomposite coatings were exposed to a thermal treatment at 150°C in air atmosphere during 30 minutes, obtaining consolidated and homogeneous films.

2.2. Structural characterization of grafted clay and coatings

In order to verify the structural condition of the starting clay nanoparticles and the effects of the silanization process, Laponite® S482 sample was observed through Scanning Electron Microscopy (SEM, Jeol 6460) in three different conditions: as received, stratified after its exfoliation in water and grafted with GPTMS. Electron microscopy was also used in order to observe the internal and superficial microstructure of coatings. Bulk microstructures of samples were observed on the transversal sections exposed through fractures mechanically performed in coatings. All the samples were previously sputtered with a thin gold–palladium film in order to improve their surface electric conductivity.

Thermogravimetric analysis (TGA Shimadzu, Series 50) was performed in order to analyse the dehydration process of Laponite® S482 and the thermal evolution of the grafted clay sample and developed coatings. Coatings were previously removed from its glass substrates by scratching. All the samples were finely powdered with an agate mortar and, then, they were analysed between 20 and 800 °C under air atmosphere at a heating rate of 10 °C/min.

X-ray powder diffraction (XRD) analysis was performed on a X-ray diffractometer (XRD, X´Pert PRO, PANalytical) equipped with a back monochromator and a copper cathode as the X-ray source (λ = 0.154 nm). The basal spacing of clay nanoparticles was determined from the 2θ values using the Bragg's equation. On the other hand, the development of silver nanoparticles and the basal spacing of clay nanoparticles in coatings were determined by X-ray diffraction with a configuration of grazing incidence (GIXRD). Diffractograms were recorded at a speed of 2 °/mm with an incidence angle of 2°. The size of silver nanoparticles developed in different coatings was determined by the Scherrer equation using a Si pattern in order to determinate the experimental width and the crystallite shape-factor approximation K=0.9.

Through the infrared absorption bands corresponding to Mg-OH bonds of clay nanosheets and to the organic components of GPTMS, the silanization process was followed by Fourier Transformed Infrared Spectroscopy (FTIR, Nicolet 6700, Thermo Scientific) with Attenuated Total Reflectance (ATR) device for Middle IR range and fiber optic probe for measurements of NIR spectra. Fiber optical waveguides were used recording spectra in the spectral ranges 400–4000 cm^{-1} and 4000–7400 cm^{-1} with a resolution of 4 cm^{-1} in both cases. An analysis of the relative intensities of the bands corresponding to the stretching vibration of Si-O-Et bond, at 1198 cm^{-1}, and to the C-O stretching of the epoxide, at 906 cm^{-1}, of GPTMS, before and after the grafting process, was used to estimate the amount of methoxy groups involved in the silanization reaction [18,19].

The effects of clay nanoparticles and silver doping, on the viscosity of the hybrid sols, were determined by measurements in a sine-wave Vibro-Viscometer (AND, SV-10 Series) by the tuning-fork vibration method. Measurements were carried out at 22°C in non-aged sols.

Effect of grafted clay on silver doped coatings was complementarily analyzed with an ultraviolet-visible spectrophotometer (UV-Vis-NIR, Shimadzu 3600Plus) equipped with integrating sphere. Spectra were recorded in absorbance mode in the wavelength range from 200 to 1000 nm, with a resolution of 1 nm, using barium sulfate as reflexivity standard.

2.3. Antibacterial performance of coatings

Antibacterial performance was qualitatively analyzed against *E. coli* in order to determine the effect of incorporation of grafted clay nanoparticles in silver enriched coatings. Cultures of *E. coli* (K12 strain RP437) were diluted 1/50 (100,000 cells/mL) and spread onto rich medium agar plates, containing 1% tryptone, 0.5% yeast extract, 0.5% NaCl and 1.3% agar. The initial bacterial concentration of the cultures was $3x10^9$ CFU/mL for all experiments. Microscope glass slides with different coatings were placed on the agar surface, and plates were incubated at 37 °C for 10 h. The inhibitory activity was visualized as a clear halo between the glass and the bacterial lawn.

3. Results and Discussion

3.1. Grafting of clay nanoparticles

Clay nanosheets were successfully grafted with a bulky organic group through a silanization process with GPTMS obtaining stable and transparent aqueous-alcoholic dispersion. This silanization process was reached following an environment-friendly method avoiding the use of strong and dry organic solvents. At neutral pH, condensation reactions prevails over hydrolysis of alkoxy groups of silanes, then, even with an excess of water, the silanization process of clay nanosheets is more expected than the hydrolysis of GPTMS.

As received, clay nanoparticles are agglomerated forming dense particles where the laminar structure is not easy to be observed under SEM, Figure 1 (a). Thus, agglomerates are present in a wide particle size distribution. As reported by the supplier, after swelling and dispersion in water, at neutral pH values, nanosheets of Laponite® S482 are easily exfoliated. The use of the phosphonate-based modifier allows to obtain highly stable dispersions and their rearrange in a dense structure after a drying process; then, instead of the *house of cards* structure, clay nanosheets are able to form a stratified structure though the stacking of clay nanoparticles, Figure 1 (b). This property is highly important in order to facilitate the grafting of clay nanosheets through a silanization process with the Mg-OH groups present in the boundaries of hectorite type sheets. Figure 1 (c) shows the stratified microstructure of clay nanoparticles exposed to the silanization process with GPTMS. This microstructure is the result of the hydrolytic condensation reactions produced between the Mg-OH groups of clay nanoparticles and the $Si\text{-}OCH_3$ groups present in GPTMS. Although the stacking phenomenon is less evident in grafted than in pure Laponite® S482, a stratified structure can be also observed under electron microscopy.

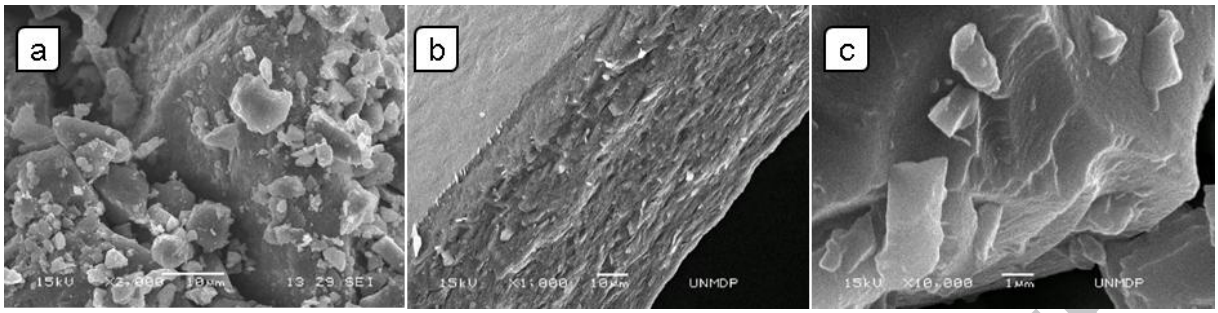

Figure 1. SEM images of Laponite® S482 (a) as received, scale bar = 10 µm; (b) after drying from dispersion in water, scale bar = 10 µm, and (c) after silanization with GPTMS, scale bar = 1 µm.

The use of a clay of synthetic origin, as Laponite® S482, avoids the introduction of different admixtures, as quartz and pyroxene, usually present in natural clays [20]. In this way, in XRD spectra of Laponite® S482, Figure 2(a), only (*001*) and (*004*) reflections, at 6.8° and 27.9°, and (*02.11*), (*20.13*) and (*06.33*) reflections, with the maxima at 19.5°, 34.7° and 60.6°, respectively, are clearly observed. In the case of grafted clay, Figure 2 (b), the XRD spectrum is dominated by a broad band attributed to an amorphous structure, and the (*001*) reflection, corresponding to the basal spacing of clay nanoparticles is observed. On the other hand, it is noticeable that none of the reflections corresponding to the crystalline structure of clay nanoparticles is observed. This phenomenon could be indicating that a range of morphologies, from disordered intercalation to exfoliation, is present [21,22]. Then, it can be assumed that, besides the silanization process of exfoliated nanoparticles, also the intercalation phenomenon is present. With the silanization process, the (*001*) reflection was shifted from 6.8° to 5.6°. By the use of the Bragg´s law it is determined that the d (*001*) basal spacing increased from 1.30 to 1.58 nm in grafted clay. This increase of basal space indicates that GPTMS molecules has been successfully grafted onto the external active sites of clay nanosheets, without a significant intercalation within the internal galleries of the clay structure that would have conducted to an spacing increase proportional to the size of the silane molecule and its arrangement [23]. In this case, after a condensation reaction in water/ethanol mixture, the silane can be attached to the active sites onto the external surface and broken-bonds edge sites of the dispersed nanoparticles of clay resulting in a structure disc-chain type arrangement that increase the basal spacing in approximately 0.28 nm. Thus, this modification in the intersheet distance, in relation with the original structure of Laponite® S482, is not enough to eliminate the Van der Waals interactions between strata and reach a totally exfoliation in the resulting dry material, but it is a simple method to functionalize the clay nanoparticles with hybrid functional chains [22,24,25].

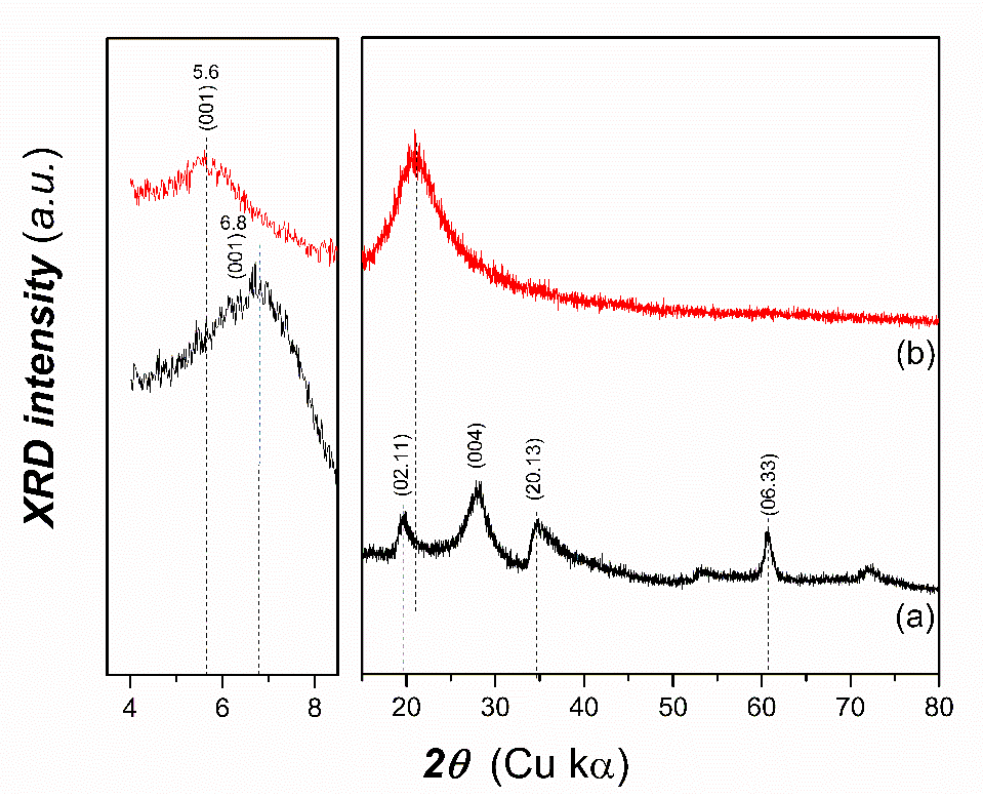

Figure 2. XRD patterns of (a) Laponite® S482 and (b) silane grafted clay.

The spectroscopic analysis through FTIR allowed corroborate the condensation reactions between Si-OR and Mg-OH groups. Figure 3 displays the infrared spectra, in near and middle regions, for (a) Laponite® S482 and (b) grafted clay; for comparative purposes, (c) GPTMS spectrum is also presented. The bands related to the Mg-OH bonds are present in the three displayed regions of the IR spectra of Laponite® S482. In the middle IR, a band at 652 cm^{-1} is attributed to the OH bending vibration (δMg_3OH) [26,27] and a broad band at 900-1050 cm^{-1} attributed to Si–O stretching vibrations of the tetrahedral sheets [28]. In the near region of the infrared spectra, IR Laponite® S482 presents several bands corresponding to a combination of bending and stretching of OH groups at 4190, 4325 and 4366 cm^{-1}, ($\nu+\delta$) OH, ($\nu+\delta$) Mg_3-OH and ($\nu+\delta$) $LiMg_2$-OH respectively, and overtones at 7194, 7218 and 7260 cm^{-1}. Overtones of the stretching vibrations of H_2O, at 6840 and 7076 cm^{-1} [29] are also observed.

After the grafting procedure, the bands attributed to the OH groups, associated to the magnesium octahedral, undergoes a strong diminution. Essentially, overtones at 7194, 7218 and 7260 cm^{-1} experience the more significant changes, being replaced by a sharp band at 7204 cm^{-1}, possibly attributed to the overtone of remnant, not reacted, structural OH groups. Additionally, a new band is observed at 7000 cm^{-1}; which is assigned to a ν(OH) overtone of hydroxyl groups related to the presence of traces of open epoxy rings [30]. As grafting takes place at neutral pH, although water is present in an abundant amount, hydrolysis of methoxy groups is not the prevailing reaction and condensation reactions occur mainly between magnesiol groups of clay nanosheets and methoxy groups of GPTMS

[31]. Then, hydrolytic condensation between GPTMS molecules is neither greatly expected. Certainly, in mid IR, the grafted clay shows a strong band at 1011 cm^{-1} and other one at 695 cm^{-1}, both attributed to the stretching vibrations of the Si-O bonds of its tetrahedral silica sheets and completely uncovered from magnesiol bands (23). Condensation of methoxy groups produces new Si-O bonds corresponding to an amorphous structure with several vibrational bands. At 1054, 1093 and 1132 cm^{-1} appear bands attributed to the transversal optic (TO) mode of the asymmetric vibration of silica, which is characteristic of energetic bonds with larger Si-O-Si angles and Si-O bond lengths [32–35]. The development of this kind of bonds is consistent with the condensation of an alkoxysilane on the magnesiol groups present in the crystalline structure, where the atoms are not able to modify their position. Certainly, the band at 1198 cm^{-1}, assigned to the stretching vibration of Si-O-Et bond of GPTMS, is still present after the grafting process. Likewise, bands at 4527 and 906 cm^{-1}, attributed to epoxy ring, are observed in grafted clay [36,37]. Considering that the epoxy groups should not undergo modification during the grafting process, its band, at 906 cm^{-1}, can be used as a reference to estimate the condensation degree of GPTMS during the process using the following equation:

$$X_f\,(\%) = 100\% \times [I_f(1198cm^{-1}) / I_f(906cm^{-1})] / [I_0(1198cm^{-1}) / I_0(906cm^{-1})] \qquad \text{Eq. 1}$$

where I_0 and I_f are the intensities, in absorbance spectra, at given wavenumbers before and after the grafting process, respectively; X_f is the resulting fraction of non-reacted methoxy groups. From spectra (*b*) and (*c*), Figure 3, ratio $I_f(1198cm^{-1})/I_f(906cm^{-1})$ = *0.82±0.01* and ratio $I_0(1198cm^{-1})/I_0(906cm^{-1})$ = *2.18±0.01*, then, it can be assumed that approximately the 38% of the methoxy groups, remains unreacted after the complete silanization process. The subsistence of residual methoxy groups could work as strong crosslinkers for further reaction with the sol-gel network through hydrolytic condensation reactions with the other alkoxy groups supplied by TEOS and GPTMS molecules. Then, the grafted GPTMS molecules on clay nanosheets, could work as coupling agent enhancing the mechanical properties of the nanocomposite material [38]. Therefore, this process of silanization, in aqueous media and neutral pH, mainly carries to the development of clay nanoparticles with their edges functionalized with epoxy groups. As a proof of the success of the synthesis, method is important to take in consideration that bands of silanol groups are not observed. The presence of Si-OH bonds should be clearly observed both at 950 and at 7300 cm^{-1} [39].

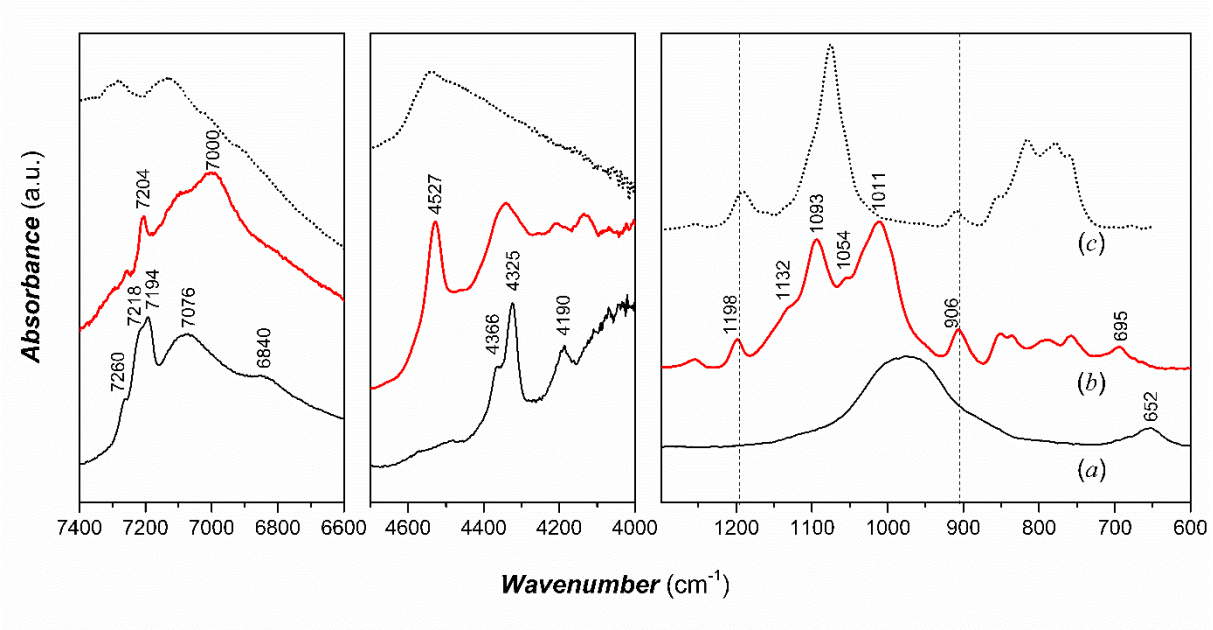

Figure 3. FTIR spectra of (a) Laponite® S482, (b) silane grafted clay and (c) GPTMS.

Thermogravimetric curve of Laponite® S482, Figure 4 (a), reveals four clear steps of weight loss, with minima, in DTG curves, at 100, 303, 483 and 760°C. The gradual weight loss at 100°C is attributed to loosening of physisorbed water, present between particles, and from the hydration sphere of exchangeable sodium cations. The minimum at 300°C is attributed to the thermal decomposition of (1-hydroxyethylidene)bisphosphonate ($C_2H_8O_7P_2{\cdot}4Na$) which is utilized as peptizing agent in Laponite® S482. Finally, the weights loosing at 483 and 760°C correspond, respectively, to the dehydroxylation process of hydroxyl groups present at the edges of platelets and from the bulk of the particles [40].

Thermogravimetric analysis of grafted clay, Figure 4 (b), shows a predictable curve for the organically grafted nanoparticles. Besides that, both samples, Laponite® S482 and grafted clay, were previously dehydrated at 100°C during 24 h; the weight losing around 100°C is certainly negligible in grafted clay. At 216°C, a sharp weight loss of 11.7 % takes place. This behaviour complies with a process of thermal decomposition of methoxy groups of GPTMS not condensed to magnesiol groups of clay nanosheets. This process of non-hydrolytic hydroxylation, thermolysis, is usually produced above 180-200°C and involves the elimination of both alkenes and water [41]. Finally, with a minimum at 300°C in DTG curve, a pronounced mass loss process is observed because of the thermal decomposition of the entire organic component. It is important take in consideration that no evidence of dehydroxylation processes, at 483 and 760°C, are observed in this sample; as it was observed in as-received Laponite® S482 sample. In grafted clay, only structural hydroxyls are not able to be condensed to silanes. Then, the absence of the weight loosing at 760 °C could be explained by the presence of degradation products, produced by thermal decomposition of GPTMS, avoiding the loosening of structural hydroxyls at the expected temperature. Thus, it is possible to assume that the grafting process was satisfactorily produced through the hydrolytic condensation of methoxy groups of GPTMS on Mg-OH groups of clay nanosheets in aqueous media at neutral pH.

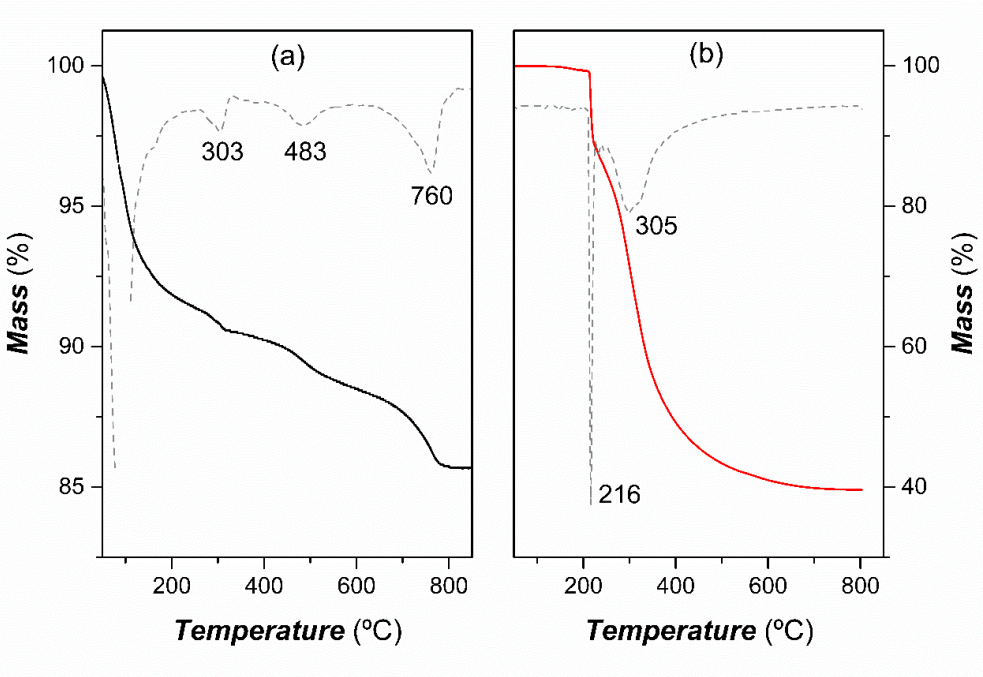

Figure 4. TGA-DTA curves of (a) Laponite® S482 and (b) silane grafted clay.

3.2. Effect of grafted clay nanoparticles in the sol-gel coatings

Grafting process of clay nanoparticles allowed its incorporation in hybrid organic-inorganic sols. Obtained sols presented an extraordinary physicochemical stability, remaining colourless, slightly translucent, and without precipitation or gelling, even after one year of storage at 4°C and light protected. Incorporation of clay nanoparticles produced a considerable increment in the viscosity, from 7.5 to values around 11.0 mPa·s both for 1 and 2 wt. %. Table 1 displays the values of viscosity of sols at 22°C. Silver doping of sols did not produce any evident change in the viscosity of sols nor at other stability parameters as changes in coloration or formation of precipitates. After deposition and thermal treatment in air atmosphere, coatings resulted transparent and cracks-free. In case of silver doping, a brownish coloration was observed in coatings.

Table 1
Viscosity values corresponding to the precursor sols at 22°C with different amounts of functionalized nanoclays.

Clay nanoparticles	**Viscosity at 22 °C** (*mPa.s*)	
(%*w/w*)	0 % Ag	3 % Ag
0	7.5 ± 0.5	7.2 ± 0.6
1	11.0 ± 0.8	11.3 ± 0.6
2	10.8 ± 0.5	11.0 ± 0.9

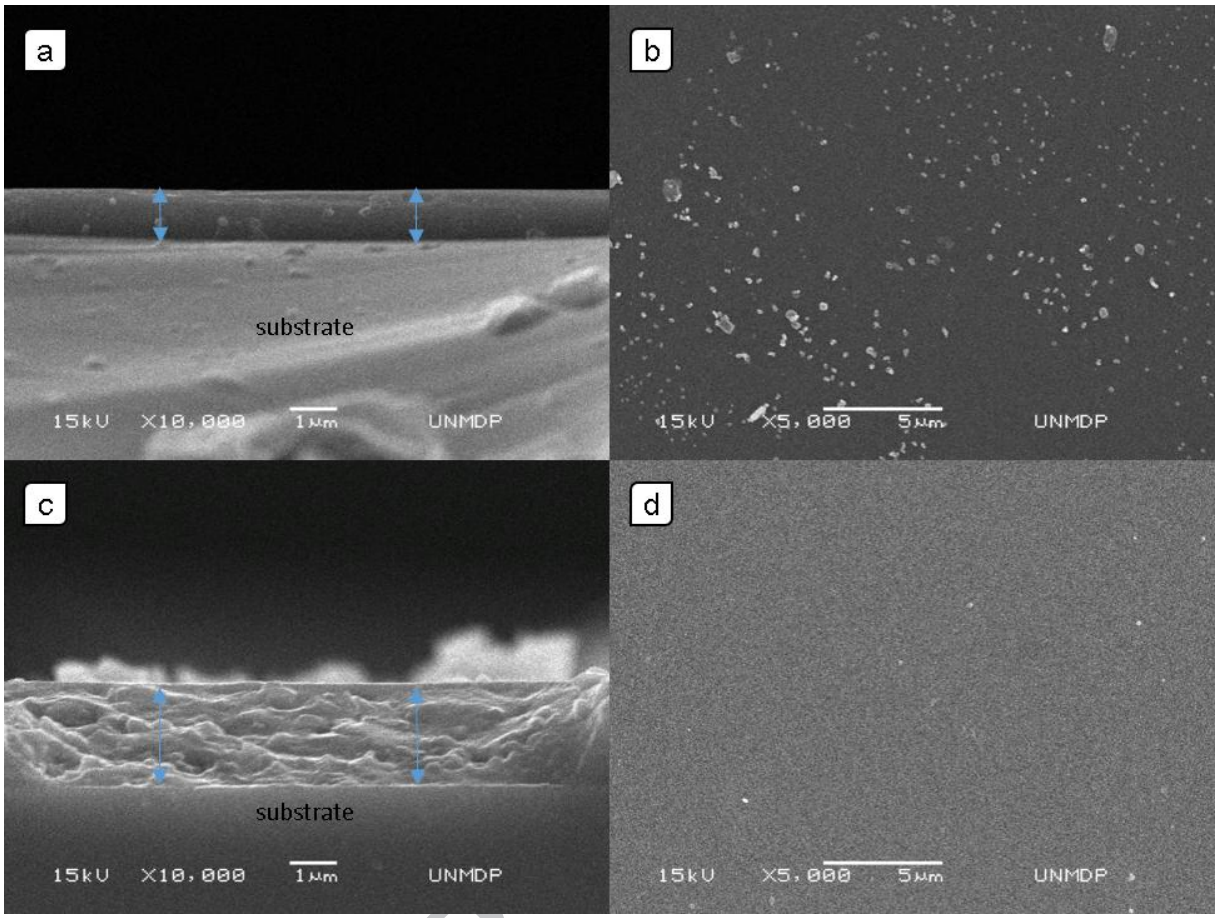

Figure 5. SEM images showing (a) the cross section and (b) the surface morphologies of TG-Ag coating; and (c) the cross section and (d) top view of TGL-Ag coating. Scale bars represent 1 µm in cross section images (X 10,000) and 5 µm in top views (X 5,000).

The increase of viscosity produced by the incorporation of clay nanoparticles into the sol formulation has a direct effect on the thickness of coatings obtained through the dip-coating method. The same withdrawal speed carried out to the development of coatings twice thicker with sols containing the grafted clay; the observed thicknesses are 1.08 ± 0.1 µm and 2.16 ± 0.1 µm for TG-Ag and TGL-Ag coatings, respectively. Figure 5 shows SEM pictures of cross-section and top of obtained TG-Ag and TGL-Ag coatings. The cross-section of the coating containing clay nanoparticles reveals a fracture surface much rougher than observed in clay-free coating; this feature could be indicative of a higher fracture toughness usually present in clay-based nanocomposite materials [42,43]. Nevertheless, the most noteworthy effect of clay in this kind of coatings is related to its interaction with the contained silver ions. In absence of any diffusion impediment, silver is free to move within the sol-gel structure towards the external surface of the coating. So, in clay-free coatings, Figure 5. (b), silver diffusion is thermally promoted and carries to the development of superficial particles in the coating surface. Although formation of silver nanoparticles could be highly required in order to give antibacterial effect at longer terms [44–46], since they are Ag^{+} reservoirs, superficial development of particles should be

strongly avoided. Differently from inner particles, the grown on the coating surface are highly exposed to detaching processes. In this sense, a relatively small amount of clay nanoparticles was enough to avoid this superficial growing of silver nanoparticles. Presumably, both the negatively charged faces of clay nanoparticles and the tortuosity introduced to the silver migration inside the sol-gel structure, played the role of to diminish, or actually to avoid, the formation of silver nanoparticles on the coating surface of TGL-Ag coating, Figure 5. (d).

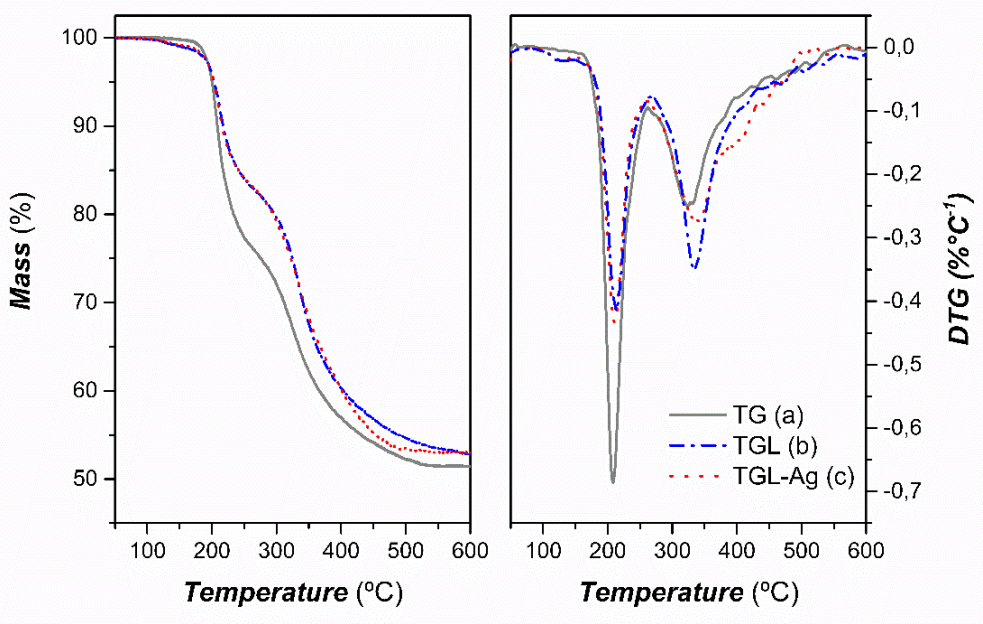

Figure 6. TGA (left) and DTG (right) curves of (a) TG, (b) TGL and (c) TGL-Ag coatings.

Thermogravimetric analysis of coatings allows to observe two main mass losing processes, Figure 6. The first one, at 216 °C, is attributed to the thermolysis process of residual Si-OR and Si-OH groups present in the hybrid matrix, and the second one, above 330°C, corresponds to the thermal degradation of glycidoxypropyl groups from GPTMS. Introduction of just 2 wt. % of Laponite® S482, in respect to condensed silica, has strong effects on the thermal behaviour of coatings. The magnitude of the thermolysis process, in terms of both mass loosening and degradation rate is considerably lower in samples containing grafted clay nanosheets, TGL and TGL-Ag samples. Certainly, the mass loses attributed to thermolysis is ≈ 13% for TGL and TGL-Ag samples and ≈ 23% for TG sample. This indicates that the presence of residual methoxy groups is near the twice in the absence of clay nanosheets. Then, the condensation degree of methoxy groups is higher when clay nanosheets are present. This phenomenon could be attributed to the preferential condensation of GPTMS on the edges of clay nanosheets during the synthesis procedure, which includes the silanization as an additional condensation process. Then, the hybrid organic-inorganic structures of coatings matrixes could be substantially different in both cases. In samples with the same TEOS/GPTMS ratio, as TG and TGL samples, the grafting process of clay nanosheets with GPTMS could carry to development of nanocomposite materials whit less organic component within their matrixes. It is important take in consideration that mass losses attributed to glycidoxypropyl groups, approximately 26% for TG sample, 32% for TGL and TGL-Ag samples and 50% for grafted clay (Figure 4) indicate that the resulting

concentration of the organic component is highly dependent on the condensation degree of methoxy groups and, then, on the presence of grafted clay nanosheets.

X-rays diffractograms of coatings, Figure 7, reveal that clay intercalation increases even more, from its silanization process. Through the sol synthesis and deposition process, the (*001*) reflection was shifted from 5.6° to 4.9°, which represent a final d(*001*) basal spacing of 1.80 nm in clay containing coatings. This final spacing reached in clay nanosheets is ascribed to the organic polymerization through the opening of epoxy rings, driving to an additional separation. On the other hand, XRD shows the peaks corresponding to the face-centered cubic (FCC) structure of silver, at 2θ = 38.2, 44.3, 64.5, and 77.4 degrees. Debye-Scherrer analysis performed on silver loaded samples, gave as result the size of silver nanocrystallites, being 28.4 ± 2.8 nm in TG-Ag samples and 21.5 ± 2.2 nm in TGL-Ag samples. This diminution of about 25 % in silver nanoparticles size could be attributed to the limitations introduced, by clay nanosheets, to the ionic diffusion. It is important to take in consideration that, presumably due to the low concentration of silver-doping, so small nanoparticles have not been clearly observed through scanning electron microscopy.

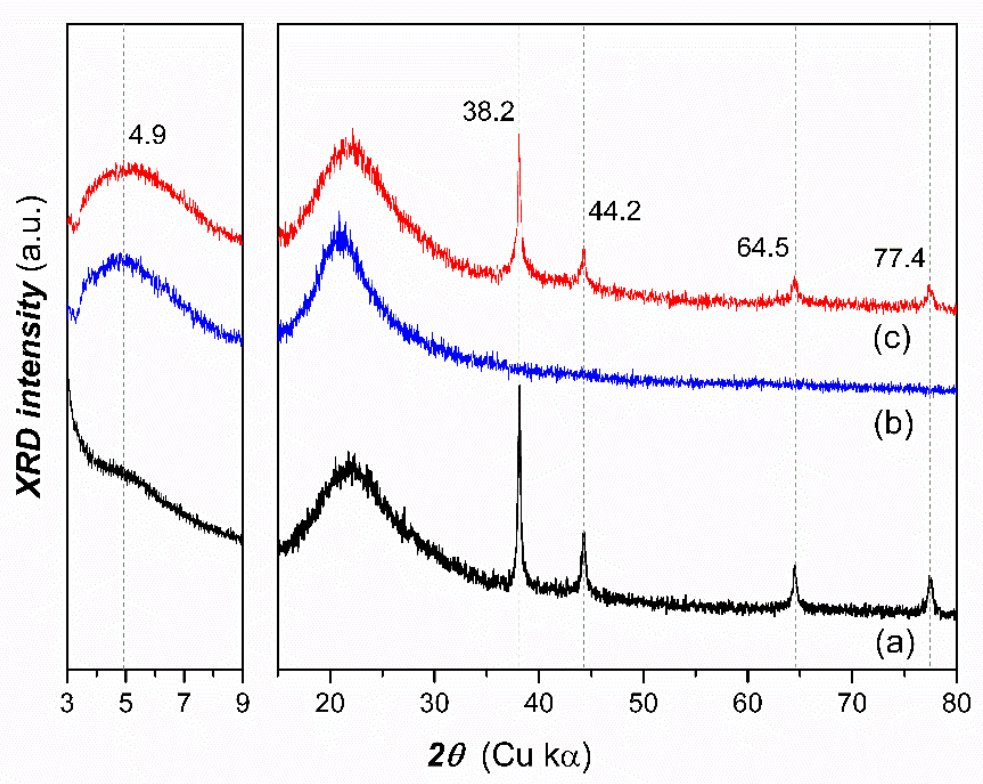

Figure 7. XRD spectra of (a) TG-Ag, (b) TGL and (c) TGL-Ag coatings.

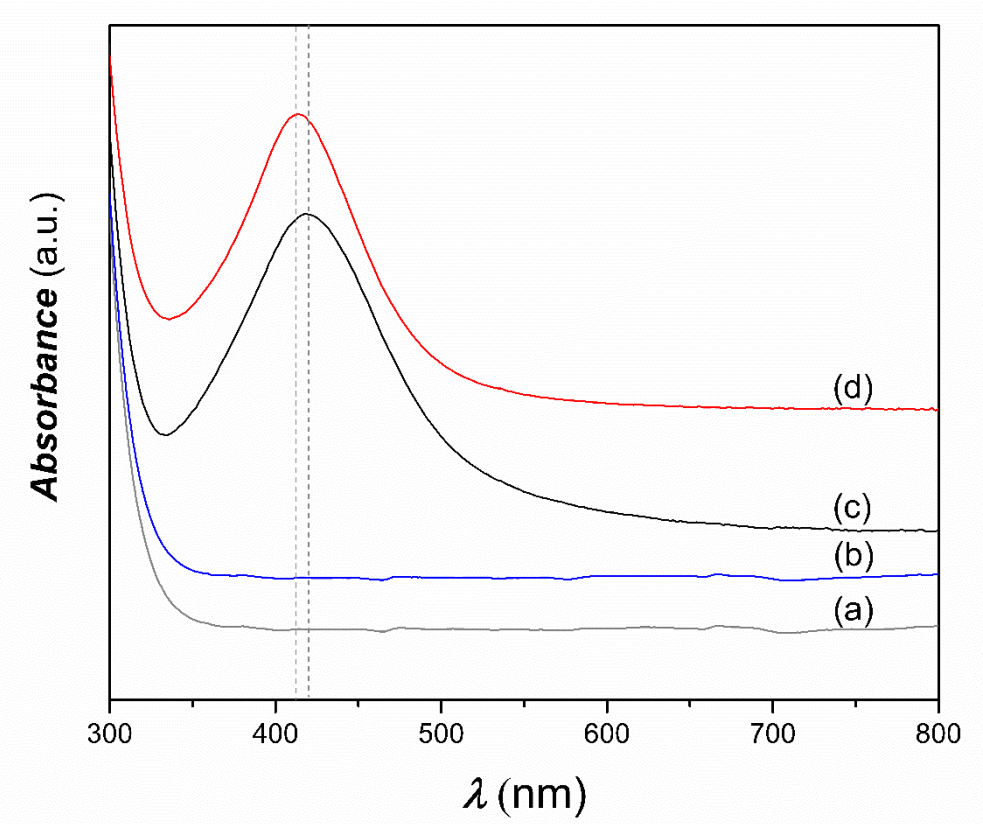

Figure 8. UV-Vis-NIR absorption spectra recorded with integrating sphere for coatings type (a) TG, (b) TGL, (c) TG-Ag and (d) TGL-Ag.

UV-VIS spectra of coatings, Figure 8, reveal the effect of clay nanoparticles on the development of silver nanoparticles from its ionic state. Besides the strong absorbance below 350 nm, attributed to silica bonds, both TG and TGL coatings present a flat spectrum in the analysed region. With the densifying thermal treatment, Ag^{+} ions reduce giving place to the development of silver nanoparticles that are clearly evidenced through its characteristic plasmonic band. In TG-Ag sample (c), silver ions can freely move through the hybrid matrix to form metallic nanoparticles and a plasmonic band was developed with a maximum at 420±1 nm. In TGL-Ag sample (d), were clay nanoparticles provide a diffusion barrier, the resulting plasmonic band was shifted towards blue, with a maximum in 414±1 nm. Although the shape and position of plasmonic bands strongly depend on the size, shape and concentration of silver nanoparticles, and on the local refractive index, the observed shift towards blue is due to a diminution in the size of developed silver nanoparticles, which is in agreement with the previously observed through XRD. Besides the blue shifting, the narrower of the plasmonic band of TGL-Ag sample reveals that the addition of grafted clay nanoparticles carried to the development of a narrower size distribution of silver nanoparticles.

3.3. Antibacterial behaviour of nanocomposite coatings

The antibacterial activity of samples was analysed against *E.-Coli* through Agar Diffusion Tests. Figure 9 shows the pictures of cultures after 10 h at 37°C for the glass slides coated with the hybrid materials. For

TG coating, with no addition of silver, bacteria colonies grown independently from the presence of the sample, while for both TG-Ag and TGL-Ag coatings the presence of an inhibitory halo was clearly observed. A qualitative analysis of the size of such inhibitory halo allows determining a clear effect of exfoliated clay nanosheets. Although it is only a qualitative visual observation, the development of inhibitory halos around samples exposed to the same bacteria inoculum, the size of such halos is directly related to the reached silver releasing rate from each sample.

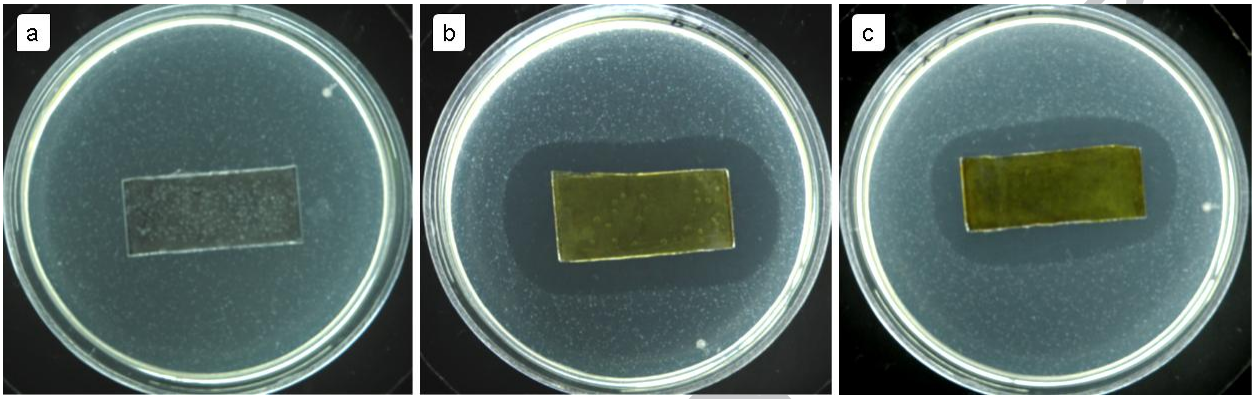

Figure 9. Agar diffusion tests performed against *E. coli* cultures on (a) TG, (b) TG-Ag and (b) TGL-Ag samples at 37 °C during 10 h.

Considering that the smaller the silver nanoparticles, the higher the behaviour against bacteria [47–49] and the difference in thickness of both silver loaded coatings, a stronger antibacterial effect could be expected on TGL-Ag coated sample. Instead, the size of its inhibitory halo is visibly lower. Nevertheless, this result is in accordance with the expected effect introduced by the organically grafted clay nanosheets. Its presence as exfoliated and highly intercalated nanoparticles offers a more tortuous pathway to the smaller clusters and silver ions, limiting their releasing towards the surface of the nanocomposite coating.

However, it is important to take in account that, although the antibacterial behaviour was verified in the developed nanocomposite coatings, a deeper study should be addressed in order to analyse the silver release kinetics and verify their antibacterial effect at longer term.

Conclusions

In this work, synthetic clay nanoparticles were organically modified with 3-glycidoxypropyl groups through a silanization process in aqueous media and incorporated in a silver-doped hybrid sol-gel formulation. Obtained sols presented a very high physicochemical stability without precipitation, gelling nor loosing of colourless upon one year at 4°C and darkness storage. While clay nanosheets where mainly exfoliated within the sol-gel matrix, an intercalation arrange was observed in coatings reaching a basal spacing up to 1.8 nm with the epoxy ring opening process. In this way, the organic polymerization process allowed to overcome the intercalation spacing obtained in wet conditions with other alkoxysilanes [9].

Although the concentration of clay nanoparticles is relatively low, they have strong effect on the structural evolution of silver within the coatings. Presence of dispersed clay nanoparticles minimized the development of silver nanoparticles at the external surface of the coating because of thermally activated diffusion of silver ions during the densifying process. Furthermore, the size distribution of silver nanoparticles reached within the sol-gel structure was considerably more uniform and smaller in case or clay incorporation. Preliminary studies performed against *E. coli* cultures suggest that microstructural properties of the developed nanocomposite coatings have a strong effect on its antibacterial performance [16]. Further studies are needed in order to verify the effect of clay nanosheets on silver releasing behaviour at longer terms.

Acknowledgments

Authors want to acknowledge the Argentine National Council of Scientific and Technical Research (CONICET, PIP 2014- 0175) for financial support. Delanta S.A. by provide the nanoclay material Laponite® S482 and Mr. Martin Lere by technical support are also acknowledged.

References

[1] M.G. Olivier, M. Fedel, V. Sciamanna, C. Vandermiers, C. Motte, M. Poelman, F. Deflorian, Study of the effect of nanoclay incorporation on the rheological properties and corrosion protection by a silane layer, Prog. Org. Coatings. 72 (2011) 15–20. doi:10.1016/j.porgcoat.2010.11.022.

[2] R. Herrera Alonso, L. Estevez, H. Lian, A. Kelarakis, E.P. Giannelis, Nafion-clay nanocomposite membranes: Morphology and properties, Polymer (Guildf). 50 (2009) 2402–2410. doi:10.1016/j.polymer.2009.03.020.

[3] F. Deflorian, S. Rossi, M. Fedel, C. Motte, Electrochemical investigation of high-performance silane sol-gel films containing clay nanoparticles, Prog. Org. Coatings. 69 (2010) 158–166. doi:10.1016/j.porgcoat.2010.04.007.

[4] W. He, D. Wu, J. Li, K. Zhang, Y. Xiang, L. Long, S. Qin, J. Yu, Q. Zhang, Surface modification of colloidal silica nanoparticles: Controlling the size and grafting process, Bull. Korean Chem. Soc. 34 (2013) 2747–2752. doi:10.5012/bkcs.2013.34.9.2747.

[5] P.A. Wheeler, J. Wang, J. Baker, L.J. Mathias, Synthesis and characterization of covalently functionalized laponite clay, Chem. Mater. 17 (2005) 3012–3018. doi:10.1021/cm050306a.

[6] I. Santana, A. Pepe, W. Schreiner, S. Pellice, S. Ceré, Hybrid sol-gel coatings containing clay nanoparticles for corrosion protection of mild steel, Electrochim. Acta. (2015). doi:10.1016/j.electacta.2016.01.214.

[7] V. Dalmoro, J.H.Z. dos Santos, E. Armelin, C. Alemán, D.S. Azambuja, Sol-gel hybrid films based on organosilane and montmorillonite for corrosion inhibition of AA2024, J. Colloid Interface Sci. 426 (2014) 308–313. doi:10.1016/j.jcis.2014.04.021.

[8] R. Naderi, M. Fedel, F. Deflorian, M. Poelman, M. Olivier, Synergistic effect of clay nanoparticles and cerium component on the corrosion behavior of eco-friendly silane sol-gel layer applied on pure aluminum, Surf. Coatings Technol. 224 (2013) 93–100. doi:10.1016/j.surfcoat.2013.03.005.

[9] N.N. Herrera, J.-M. Letoffe, J.-P. Reymond, E. Bourgeat-Lami, Silylation of laponite clay particles with monofunctional and trifunctional vinyl alkoxysilanes, J. Mater. Chem. 15 (2005) 863. doi:10.1039/b415618h.

[10] N.N. Herrera, J.M. Letoffe, J.L. Putaux, L. David, E. Bourgeat-Lami, Aqueous dispersions of silane-functionalized laponite clay platelets. A first step toward the elaboration of water-based polymer/clay nanocomposites, Langmuir. 20 (2004) 1564–1571. doi:10.1021/la0349267.

[11] A.M. Shanmugharaj, K.Y. Rhee, S.H. Ryu, Influence of dispersing medium on grafting of aminopropyltriethoxysilane in swelling clay materials, J. Colloid Interface Sci. 298 (2006) 854–859. doi:10.1016/j.jcis.2005.12.049.

[12] M. Rai, A. Yadav, A. Gade, Silver nanoparticles as a new generation of antimicrobials, Biotechnol. Adv. 27 (2009) 76–83. doi:10.1016/j.biotechadv.2008.09.002.

[13] R. Procaccini, A. Bouchet, J.I. Pastore, C. Studdert, S. Cer??, S. Pellice, Silver-functionalized methyl-silica hybrid materials as antibacterial coatings on surgical-grade stainless steel, Prog. Org. Coatings. 97 (2016) 28–36. doi:10.1016/j.porgcoat.2016.03.012.

[14] R.A. Procaccini, C.A. Studdert, S.A. Pellice, Silver doped silica-methyl hybrid coatings. Structural evolution and antibacterial properties, Surf. Coatings Technol. 244 (2014) 92–97. doi:10.1016/j.surfcoat.2014.01.036.

[15] R. Procaccini, S. Ceré, S. Pellice, Development and thermal evolution of silver clusters in hybrid organic-inorganic sol-gel coatings, Surf. Coatings Technol. 205 (2011) 5464–5469. doi:10.1016/j.surfcoat.2011.06.018.

[16] H. Miyoshi, H. Ohno, K. Sakai, N. Okamura, H. Kourai, Characterization and photochemical and antibacterial properties of highly stable silver nanoparticles prepared on montmorillonite clay in n-hexanol, J. Colloid Interface Sci. 345 (2010) 433–441. doi:10.1016/j.jcis.2010.01.034.

[17] B. Brunier, N. Sheibat-Othman, M. Chniguir, Y. Chevalier, E. Bourgeat-Lami, Investigation of Four Different Laponite Clays as Stabilizers in Pickering Emulsion Polymerization, Langmuir. 32 (2016) 6046–6057. doi:10.1021/acs.langmuir.6b01080.

[18] P. Innocenzi, C. Figus, M. Takahashi, M. Piccinini, L. Malfatti, Structural evolution during evaporation of a 3-glycidoxypropyltrimethoxysilane film studied in situ by time resolved infrared spectroscopy., J. Phys. Chem. A. 115 (2011) 10438–44. doi:10.1021/jp204314b.

[19] I.M. Šapić, L. Bistričić, V. Volovšek, V. Dananić, K. Furić, DFT study of molecular structure and vibrations of 3-glycidoxypropyltrimethoxysilane, Spectrochim. Acta - Part A Mol. Biomol. Spectrosc. 72 (2009) 833–840. doi:10.1016/j.saa.2008.11.032.

[20] S.J. Chipera, D.L. Bish, Baseline studies of the clay minerals society source clays: Powder X-ray diffraction analyses, Clays Clay Miner. 49 (2001) 398–409. doi:10.1346/CCMN.2001.0490511.

[21] G.K. Serhatkulu, S.E. Horsch, R. Kannan, E. Gulari, Structure and Rheology of Supercritical Carbon Dioxide Exfoliated Polymer Nanocomposites, NSTI-Nanotech. 2 (2005) 123–126.

[22] T. Lan, P.D. Kaviratna, T.J. Pinnavaia, Mechanism of Clay Tactoid Exfoliation in Epoxy-Clay Nanocomposites, Chem. Mater. 7 (1995) 2144–2150. doi:10.1021/cm00059a023.

[23] L. Mercier, T.J. Pinnavaia, A functionalized porous clay heterostructure for heavy metal ion (Hg2+) trapping, Microporous Mesoporous Mater. 20 (1998) 101–106. doi:10.1016/S1387-1811(97)00019-X.

[24] M. Park, I.K. Shim, E.Y. Jung, J.H. Choy, Modification of external surface of laponite by silane grafting, J. Phys. Chem. Solids. 65 (2004) 499–501. doi:10.1016/j.jpcs.2003.10.031.

[25] H. He, J. Duchet, J. Galy, J.F. Gerard, Grafting of swelling clay materials with 3-aminopropyltriethoxysilane, J. Colloid Interface Sci. 288 (2005) 171–176. doi:10.1016/j.jcis.2005.02.092.

[26] H. Pálková, J. Madejová, M. Zimowska, E.M. Serwicka, Laponite-derived porous clay heterostructures: II. FTIR study of the structure evolution, Microporous Mesoporous Mater. 127 (2010) 237–244. doi:10.1016/j.micromeso.2009.07.012.

[27] V.C. Farmer, Infrared Spectroscopy in Clay Mineral Studies, Clay Miner. 7 (1968) 373–387. doi:10.1180/claymin.1968.007.4.01.

[28] J. Madejová, M. Pentrák, H. Pálková, P. Komadel, Near-infrared spectroscopy: A powerful tool in studies of acid-treated clay minerals, Vib. Spectrosc. 49 (2009) 211–218. doi:10.1016/j.vibspec.2008.08.001.

[29] J. Madejová, Ľ. Jankovič, M. Pentrák, P. Komadel, Benefits of near-infrared spectroscopy for characterization of selected organo-montmorillonites, Vib. Spectrosc. 57 (2011) 8–14. doi:10.1016/j.vibspec.2011.04.001.

[30] P. Musto, M. Abbate, G. Ragosta, G. Scarinzi, A study by Raman, near-infrared and dynamic-mechanical spectroscopies on the curing behaviour, molecular structure and viscoelastic properties of epoxy/anhydride networks, Polymer (Guildf). 48 (2007) 3703–3716. doi:10.1016/j.polymer.2007.04.042.

[31] C. Brinker, G. Scherer, Sol-Gel Science: The Physics and Chemistry of Sol-Gel Processing, Adv. Mater. 3 (1990) 912. doi:10.1186/1471-2105-8-444.

[32] C.M. Bertelsen, F.J. Boerio, Linking mechanical properties of silanes to their chemical structure: An analytical study of ??-GPS solutions and films, Prog. Org. Coatings. 41 (2001) 239–246. doi:10.1016/S0300-9440(01)00135-7.

[33] S.K. Medda, D. Kundu, G. De, Inorganic-organic hybrid coatings on polycarbonate. Spectroscopic studies on the simultaneous polymerizations of methacrylate and silica networks, J. Non. Cryst. Solids. 318 (2003) 149–156. doi:10.1016/S0022-3093(02)01862-8.

[34] N. Viart, J.L. Rehspringer, Study of the action of formamide on the evolution of a sol by pH measurements and Fourier transformed infra-red spectroscopy, J. Non. Cryst. Solids. 195 (1996) 223–231. doi:10.1016/0022-3093(95)00540-4.

[35] Z. Sassi, J.C. Bureau, A. Bakkali, Spectroscopic study of TMOS ± TMSM ± MMA gels Previously identi ® cation of the networks inside the hybrid material, 28 (2002) 299–318.

[36] G.A. George, P. Cole-Clarke, N. St. John, G. Friend, Real-time monitoring of the cure reaction of a TGDDM/DDS epoxy resin using fiber optic FT-IR, J. Appl. Polym. Sci. 42 (1991) 643–657. doi:10.1002/app.1991.070420310.

[37] M. González-González, J.C. Cabanelas, J. Baselga, Applications of FTIR on Epoxy Resins - Identification, Monitoring the Curing Process, Phase Separation and Water Uptake, Univ. Carlos III Madrid. 2 (2012) 261–284. doi:10.5772/2055.

[38] E.P. Plueddemann, Reminiscing on silane coupling agents, J. Adhes. Sci. Technol. 5 (1991) 261–277. doi:10.1163/156856191X00350.

[39] A. a Christy, P.K. Egeberg, Quantitative determination of surface silanol groups in silicagel by deuterium exchange combined with infrared spectroscopy and chemometrics., Analyst. 130 (2005) 738–744. doi:10.1039/b501895c.

[40] H. Pálková, J. Madejová, M. Zimowska, E. Bielańska, Z. Olejniczak, L. Lityńska-Dobrzyńska, E.M. Serwicka, Laponite-derived porous clay heterostructures: I. Synthesis and physicochemical characterization, Microporous Mesoporous Mater. 127 (2010) 228–236. doi:10.1016/j.micromeso.2009.07.019.

[41] D.P. Debecker, V. Hulea, P.H. Mutin, Mesoporous mixed oxide catalysts via non-hydrolytic sol-gel: A review, Appl. Catal. A Gen. 451 (2013) 192–206. doi:10.1016/j.apcata.2012.11.002.

[42] A.S. Zerda, A.J. Lesser, Intercalated clay nanocomposites: Morphology, mechanics, and fracture behavior, J. Polym. Sci.

Part B Polym. Phys. 39 (2001) 1137–1146. doi:10.1002/polb.1090.

[43] K. Wang, L. Chen, J. Wu, M.L. Toh, C. He, A.F. Yee, Epoxy nanocomposites with highly exfoliated clay: Mechanical properties and fracture mechanisms, Macromolecules. 38 (2005) 788–800. doi:10.1021/ma048465n.

[44] G. Franci, A. Falanga, S. Galdiero, L. Palomba, M. Rai, G. Morelli, M. Galdiero, Silver nanoparticles as potential antibacterial agents, Molecules. 20 (2015) 8856–8874. doi:10.3390/molecules20058856.

[45] J.S. Kim, E. Kuk, K.N. Yu, J.H. Kim, S.J. Park, H.J. Lee, S.H. Kim, Y.K. Park, Y.H. Park, C.Y. Hwang, Y.K. Kim, Y.S. Lee, D.H. Jeong, M.H. Cho, Antimicrobial effects of silver nanoparticles, Nanomedicine Nanotechnology, Biol. Med. 3 (2007) 95–101. doi:10.1016/j.nano.2006.12.001.

[46] A. Panáček, L. Kvítek, R. Prucek, M. Kolář, R. Večeřová, N. Pizúrová, V.K. Sharma, T. Nevěčná, R. Zbořil, Silver colloid nanoparticles: Synthesis, characterization, and their antibacterial activity, J. Phys. Chem. B. 110 (2006). doi:10.1021/jp063826h.

[47] J.R. Morones, J.L. Elechiguerra, A. Camacho, K. Holt, J.B. Kouri, J.T. Ramírez, M.J. Yacaman, The bactericidal effect of silver nanoparticles, Nanotechnology. 16 (2005) 2346–2353. doi:10.1088/0957-4484/16/10/059.

[48] V. Dal Lago, L. França de Oliveira, K. de Almeida Gonçalves, J. Kobarg, M. Borba Cardoso, Size-selective silver nanoparticles: future of biomedical devices with enhanced bactericidal properties, J. Mater. Chem. 21 (2011) 12267. doi:10.1039/c1jm12297e.

[49] G.A. Martínez-Castañón, N. Niño-Martínez, F. Martínez-Gutierrez, J.R. Martínez-Mendoza, F. Ruiz, Synthesis and antibacterial activity of silver nanoparticles with different sizes, J. Nanoparticle Res. 10 (2008) 1343–1348. doi:10.1007/s11051-008-9428-6.